Global interactions between feature-based and spatial attention redistribute feature sensitivity across visual space

D.M. van Es J. Theeuwes T. Knapen

- Affiliation (all authors)
  - Behavioral and Movement Sciences, Vrije Universiteit Amsterdam, 1081 BT Amsterdam, the Netherlands
- Corresponding Author:
  - T. Knapen
  - tknapen@gmail.com

- Quantities
  - pages: 42, figures: 7, tables: 7,
  - abstract: 249 words, introduction: 584 words, discussion: 1500 words
- Conflict of interest
  - The authors declare no competing financial interests.
- Abbreviated title:
  - Feature-based & spatial attention in visual cortex

Abstract

Sensitivity for different visual features is not evenly distributed across visual space. However, the sampling of visual space is not fixed: attending a location in space is thought to increase spatial resolution by shifting receptive fields towards the attended location. Here, we investigated whether such changes in the sampling of visual space lead to a concurrent redistribution of feature sensitivities across the visual field and whether these changes depend on the attended feature.

To this purpose, we estimated voxels' spatial sampling in 5 human subjects under conditions of differential spatial and feature-based attention. Specifically, participants either performed a task at fixation, or on the color or temporal frequency content of a visual stimulus. We also recorded each voxel's relative response modulation to changes in color and temporal frequency information.

Directing spatial attention towards the mapping stimulus altered population receptive field (pRF) size and eccentricity in concert. This resampling of visual space was more pronounced when attending the stimulus' color compared to temporal frequency content throughout the visual system. This effect was best modeled using an attention field model in which the attention field spread was similar across all visual field maps, and smaller when attending the stimulus' color. In higher visual cortex these changes optimized feature sampling for task demands by alleviating a relatively low preference for color in the periphery.

Together, these results show that spatial and feature-based attention interact in order to redistribute both spatial and featural processing resources across the visual field depending on task demands.

Significance statement

Sensitivity to visual features is not evenly distributed across visual space, as color compared to temporal frequency sensitivity is higher near the fovea. Spatial attention changes the sampling of visual space in order to better represent the attended location. We show that feature-based attention leverages this spatial resampling in order to redistribute fea-

ture processing resources across visual space. These results outline novel, intricate interactions between spatial and feature-based attentional modulations of visual representations.

Introduction

The resolution of the visual system is highest at the fovea and decreases gradually with increasing eccentricity. But the visual system's resolution is not fixed. Attention can be directed to a location in space and/or a visual feature, which temporarily improves perceptual sensitivity (Posner et al., 1980; Rossi and Paradiso, 1995; Found and Müller, 1996; Carrasco and Yeshurun, 1998; Yeshurun and Carrasco, 1999; Kumada, 2001; Saenz et al., 2003; Wolfe et al., 2003; Theeuwes and Van der Burg, 2007) at the cost of reduced sensitivity for non-attended locations and features (Pestilli and Carrasco, 2005; Wegener et al., 2008).

The visual resolution hypothesis (Anton-Erxleben and Carrasco, 2013) posits that spatial attention improves visual resolution by changing receptive fields (RFs) to better sample the attended location. Indeed, electrophysiological studies have demonstrated that RFs shift towards an attended location in macaque MT+ (Womelsdorf et al., 2006) and V4 (Connor et al., 1997). Using fMRI to measure population receptive fields (pRFs), it was shown that such attention induced pRF shifts occur throughout human visual cortex, starting as early as area V1 and becoming progressively stronger along the visual hierarchy (Klein et al., 2014; Kay et al., 2015; Sheremata and Silver, 2015; Vo et al., 2017).

Feature-based attention selectively increases activity in those units (i.e. voxels/neurons) that represent the attended feature, irrespective of the attended stimulus's spatial location, as evidenced by both fMRI (Saenz et al., 2002; Serences and Boynton, 2007; Jehee et al., 2011) and electrophysiological (Treue and Maunsell, 1996, 1999; McAdams and Maunsell, 2000; Maunsell and Treue, 2006; Müller et al., 2006; Zhang and Luck, 2009; Zhou and Desimone, 2011) studies. However, like spatial resolution, the distribution of feature sensitivities across the visual field is not uniform. For example, sensitivity to color versus temporal information is relatively high near the fovea. This is manifested already in the retina (Curcio et al., 1990), in projections to V1 (Azzopardi et al., 1999), in extra-striate areas (Brewer et al., 2005; Lui et al., 2007), and persists into behavior (Hartmann et al., 1979; McKee and Nakayama, 1984; Hansen et al., 2009).

Here, we investigated the interaction between feature-based and spatial attention, focusing on their redistribution of visual processing resources. We hypothesize that feature-

based attention redistributes feature-processing resources akin to how spatial attention redistributes spatial processing resources. Specifically, to capture the interaction of feature-based and spatial attention we extend the visual resolution hypothesis (Anton-Erxleben and Carrasco, 2013) by proposing that *feature-specific spatial attention* serves to simultaneously improve sensitivity for the attended stimulus's spatial and featural information. That is, changes in the way space is represented in visual cortex should depend on 1. the attended location, 2. the attended feature at that location and 3. the distribution of feature sensitivity across the visual field.

We estimated voxels' pRFs under conditions of differential spatial and feature-based attention: participants either performed a task at fixation, or on the color or temporal frequency content of a visual stimulus. Importantly, visual stimulation did not differ between these attention conditions. This design allowed us to compare spatial responses to different feature-based and spatial attention conditions. Furthermore, we characterised each voxels' relative activation to changes of a full-field stimulus's temporal frequency and color content. This experiment allowed us to investigate changes in the spatial tuning of voxels resulting from the manipulation of both spatial and feature-based attention as a function of their feature preferences.

Materials and Methods

Participants

Five participants (2 female, 2 authors, aged between 25 - 37) participated in the study. All gave informed consent, according to ethical approval granted by the Vrije Universiteit Amsterdam.

Apparatus

MRI acquisition

All MRI data was acquired on a Philips Achieva 3T scanner (Philips Medical Systems), equipped with a 32-channel head coil. T1 weighted images were acquired for each subject with isotropic resolution of 1 mm^3, repetition time (TR) of 8000 ms, TE of 3.73 ms, flip angle of 8°. Functional T2* weighted data consisted of 30 2D slices of echo planar images

(EPI) with isotropic resolution of 2.5 mm^2, with a 0.25 mm slice gap, TR of 1600 ms, TE of 27.62 ms, and a flip angle of 70°. Each subject completed between 6 to 8 Attention-pRF Mapping runs (20 min each) and 2-3 Stimulus Mapper runs (10 min each), spread over 2 (N = 1) or 3 (N = 4) sessions within a 2 week period (see Experimental Design and Statistics).

Gaze recording

During all functional runs, gaze position was recorded using an Eyelink 1000 (SR Research, Osgoode, Ontario, Canada), sampled at 1000 Hz. A 9-point calibration-validation procedure was run at the start of each session.

Stimulus presentation

Visual stimuli were created in PsychoPy (Peirce, 2008) and run on a 15 inch 2013 MacBook Pro Retina. Participants viewed a 32 inch BOLD screen (resolution: 1920 x 1080, refresh rate: 100 Hz; Cambridge Research Systems), at 156 cm distance of the participants' eyes, through a gamma linear mirror. Auditory stimuli were presented through headphones using the MRConfon system.

Experimental Design and Statistics

Attention-PRF Mapping Stimulus

A bar stimulus of 0.9 degrees of visual angle (dva) width traversed a circular aperture of 7.2 dva in one of eight directions (cardinal and diagonal orientations in both directions, see Figure 1A), completing a full pass in 38.4 s by stepping 0.34 dva every 1.6 s, and pausing 3.2 s between each bar pass. One run contained 24 bar passes in total (3 for every direction), plus four blank periods of 38.4 s when no bar stimulus was shown. Throughout the experiment, a gray disk of 9.6 arcmin (60 cd/m^2), with a 4.2 arcmin dark-gray rim (0 cd/m^2) was present on the screen as a fixation mark. The bar stimulus was composed of 1500 Gabor elements (4.34 cycle/dva spatial frequency, 9 arcmin sd, average luminance of 60 cd/m^2) projected over a dark-gray background (15 cd/m^2). Three times per bar location (i.e. every 533 ms), Gabor element parameters were updated to a new random location (uniformly distributed over the spatial extent of the bar at full width),

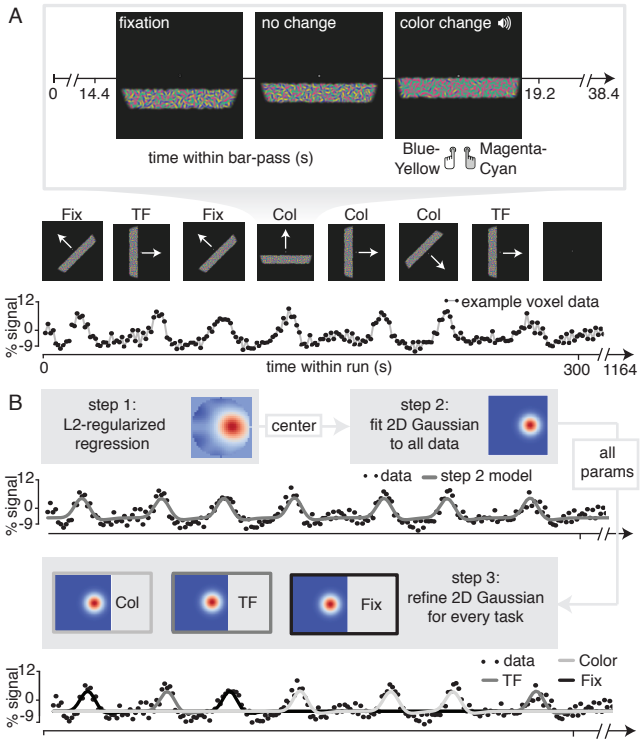

Figure 1: Experimental Design and pRF Fitting procedure. A. Experimental Design. Participants reported either changes in color (*Attend Color*) or temporal frequency (*Attend TF*) of Gabor elements within the moving bar stimulus, or changes in fixation mark luminance (*Attend Fixation*), while maintaining accurate fixation. Participants were informed auditorily about the upcoming task 2 s before each bar pass. B. Overview of pRF fitting procedure. pRF parameters were estimated from each voxel's BOLD signal time course in a three step procedure. First, a design matrix was constructed based on 1021 pixels' visual stimulation time course of the entire experiment, which was convolved with a subject-specific HRF. L2-regularized regression was used to find the position of the spatial response profile's peak of each voxel. Second, to find precise estimates of pRF center location and size we used gradient descent to fit a single parameterized 2D Gaussian pRF model with x, y parameters for all attention conditions combined, initialized at the L2-regression derived location. Third, 2D Gaussian pRF models were fitted for the different attention conditions separately, intialized with the parameters resulting from step 2.

a random orientation (uniformly drawn between 0 - 360°), a random color combination (either blue-yellow (BY), or cyan-magenta (CM)) and a random new temporal frequency (either high or low). The high and low temporal frequencies were chosen per participant to facilitate their ability to distinguish TF changes (6 and 4 Hz in 3 participants, 3 and 7 Hz in 2 participants). The overal color and/or temporal frequency composition of the bar was transiently altered on some of these parameter updates, by changing the ratio of Gabor elements assigned either color combination or either temporal frequency (as targets for the behavioral tasks, see below). The temporal predictability of these events was minimized by randomly drawing occurences according to an exponential distribution (mean 4 s, minimum 2 s). Additionally, the fixation mark central disk luminance either increased or decreased, with probability and duration of these occurrences identical to those of changes in the bar stimulus composition. These three types of transients (fixation mark luminance, bar color and temporal frequency composition) were independent, meaning they were randomly interleaved and could be combined on the screen. Importantly, this design ensured that physical stimulation was equated across all three attention conditions, which we describe below.

Attention-PRF Mapping Task

For an overview of the stimulus and behavioral task, see Figure 1A. Before each bar pass an automated voice (Apple OSX Dictation voice 'Kathy') informed participants to perform a 2-alternative forced-choice task (2AFC) on one of the three stimulus parameter deviations. Task-relevant visual stimulus changes were accompanied by an auditory pure tone (440 Hz). This auditory cue alerted the participant to respond, while task-irrelevant stimulus changes occurred independently and without warning tone. This ensured that all task-related information was conveyed to the participant by auditory means, without concurrent changes in visual stimulation. In the *Attend Color* condition, participants judged the relative predominance of Blue-Yellow or Cyan-Magenta Gabor elements in the bar stimulus, while in the *Attend TF* condition, participants judged the relative predominance of high compared to low temporal frequency Gabor elements in the bar stimulus. In the *Attend Fixation* condition, participants judged whether the central disk of the fixation mark increased or decreased in luminance. The magnitude of the stimulus changes

titrated by means of a Quest staircase procedure (Watson and Pelli, 1983), set to approximate 83% correct performance. In order to equate task difficulty across conditions and bar stimulus eccentricity, we used separate Quest staircases at three different bar stimulus eccentricies in each of the attention conditions. Additionally, there was a separate staircase for the *Attend Fixation* task when no bar stimulus on screen. This made a total of 10 separate staircases during the experiment. Participants extensively practiced the task outside the scanner and staircases were reset before scanning. Each experimental run contained one bar pass per task condition, per direction, in random order (total of 24 bar passes per run).

Feature preference (and HRF) Mapper

We performed a separate randomised fast event-related fMRI experiment in order to (1) determine each voxels' relative preference for Color and TF, and (2) to find the parameters that best described each participants' HRF, to be used in the pRF estimation procedure (see below). Full-field stimuli consisted of 8000 Gabor elements, uniformly distributed throughout the full circular aperture traversed by the pRF mapping stimulus ensuring identical density compared to the Attention-pRF Mapping stimulus. Also, every 533 ms, all Gabor elements were assigned a new random orientation and location. These stimuli were presented for 3.2 s, with an inter-trial interval of 3.2 s. In a full factorial 2 x 2 design, we varied the color and temporal frequency content of the stimulus in an on-off fashion. That is, the temporal frequency of the Gabor elements was either 0 or 7 Hz, and the elements were either grayscale or colored (balanced BY/CM). Trial order was determined based on an M-sequence (Buračas and Boynton, 2002), with no-stimulus (null) trials interspersed as a fifth category of trials. During this experiment, participants performed the same 2-AFC fixation-point luminance task as in the Attention-PRF Mapping Task (*Attend Fixation*), using a separate staircase. A single HRF was determined per subject using the R1-GLM approach (Pedregosa et al., 2015), on data from all conditions. The median HRF from the 1000 most responsive voxels (highest beta-weights in the colored high temporal frequency condition) was used as the subject specific HRF.

MRI Preprocessing

T1-weighted images were first segmented automatically using Freesurfer, after which the pial and grey/white matter surfaces were hand-edited. For every participant, one session's EPI image was selected as the target EPI, which was registered to his/her Freesurfer segmented T1-weighted image using the bbregister utility, after which the registration was hand-adjusted. Then, all EPI images were first motion corrected to their middle volume using FSL (Jenkinson et al., 2012) MCFLIRT to correct for within run motion. Then, all EPI images were registered both linearly (using FLIRT) and non-linearly (using FNIRT) to the mean-motion corrected target EPI to correct for between run and session motion and inhomogeneities in B0 field. Low frequency drifts were removed using a 3rd order savitzky-golay filter (Savitzky and Golay, 1964) with a window length of 120s. Arbitrary BOLD units were converted to percent-signal change on a per-run basis.

pRF fitting procedure

We approximated the pRF by a two-dimensional isotropic Gaussian function. For an overview of our pRF fitting procedure, see Figure 1B. A predicted timecourse for a given Gaussian function can be created by first computing the overlap of this function with a model of the stimulus for each timepoint, and then convolving this overlap with the subject-specific HRF (Dumoulin and Wandell, 2008). It is possible to find these Gaussian parameter estimates using a minimization algorithm, but such an approach is at risk of missing the global optimum when parameters are not initialized at appropriate values. Recently, a model-free reverse-correlation-like method was developed, generating a pRF spatial profile without requiring any pre-set parameters (for details see Lee et al. (2013)). Briefly, this was achieved using L2 regularised (Ridge) regression on a subject-specific-HRF convolved design matrix coding the stimulus position in a 31x31 grid for each timepoint, predicting data from all attention conditions together. Using a high regularisation parameter ($\lambda = 10^6$), we used this procedure not to maximize explained signal variance, but to robustly determine the pRF center, which was defined as the position of the maximum weight. Having determined these approximate initial values for the pRF center, we next initialized a minimization procedure (Powell (1964) algorithm) at these location values, fitting position (x, y), size, baseline and amplitude parameters of an isotropic 2D Gaussian to data from all conditions together. Then, all resulting Gaussian parameters

were used to initialize a second minization procedure which fitted a Gaussian for each attention condition separately at the same time (all parameters independent except for one shared baseline parameter). This approach allowed us to recover fine-grained differences in pRF parameters under conditions of differential attention.

pRF selection

We discarded pRFs that were either at the edge of the stimulus region (above 3.3 dva in the *Attend Fixation* condition), or had size (standard deviation) larger than our stimulus diameter (7.2 dva) in any of the tasks. Additionally, each voxel's contribution to all analyses was weighted according to the quality of fit of the pRF model, which was defined as 1 minus the ratio of residual to observed variance:

$$R^2 = 1 - \frac{\sum_i (m_i - p_i)^2}{\sum_i (m_i - \bar{m}_i)^2} \quad (1)$$

where i, m and p refer to voxel index, measured BOLD time-course and predicted time-course respectively. We disregarded voxels with an $R^2 < .1$. In order to investigate the effect of spatial attention regardless of feature-based attention, a separate *Attend Stimulus* meta-condition was created by averaging pRF parameters between the *Attend Color* and *Attend TF* conditions.

pRF parameter analyses

For the pRF parameter analyses p-values and confidence intervals were computed using 10^5 fold bootstrap procedures. For the selection of ROIs (Figure 2A), resampling was performed across participants. For all other analyses, voxels were pooled across participants and resampling was performed across voxels. To test whether bootstrapped distributions differed from a certain threshold p-values were defined as the ratio of bootstrap samples below versus above that threshold multiplied by 2 (all reported p-values are two-tailed). Outliers were determined using a threshold of five two-sided median absolute deviations and were subsequently excluded from analyses. Outlier rejection was performed either per visual field bin (cf. Figure 3B), per eccentricity bin (cf. Figures 2B, Figures 3D, 4A, B, C(scatter plot), 6A) or per ROI (cf. Figures 3C, 4C(correlation), 6B, C). When computing correlations across voxels using the Mapper β values (cf. Figures 6C),

these β values were first z-scored per participant per ROI before pooling across participants. When comparing correlations to either 0 or between conditions, correlations were Fisher transformed using the inverse hyperbolic tangent function.

Feature attention modulation index

We computed a per-voxel index for how strongly feature based attention modulated the effects of spatial attention (feature attention modulation index, or feature AMI). This measure combined pRF eccentricity and size parameters, as our results showed that spatial attention affected these parameters in concert (see 4). Per voxel and per attention condition to the bar stimulus, (*Attend Stimulus*, *Attend Color*, and *Attend TF*) we set up a two-dimensional vector comprising the difference in pRF eccentricity and size relative to the *Attend Fixation* condition. To express modulations of differential feature-based attention in terms of spatial resampling induced by differential spatial attention, we projected the *Attend Color* and *Attend TF* vectors onto the *Attend Stimulus* vector. These projections were then converted to a feature AMI through dividing their difference by their sum. This way, positive values of feature AMI indicate greater spatial attention effects on pRF parameters in the *Attend Color* condition than in the *Attend TF* condition and vice versa. Note that this measure abstracted out both the affected pRF parameter (i.e. eccentricity and size) and the sign of these changes.

Attention Field modeling

Our model represents the measured Gaussian pRF as the multiplication between a Gaussian stimulus-driven pRF (*SD*, i.e. the pRF outside the influence of attention), and a Gaussian Attention Field (*AF*; Reynolds and Heeger (2009), Womelsdorf et al. (2008), Klein et al. (2014)). Decreasing AF width results in increased pRF shift magnitude, akin to a more focused 'spotlight' of attention. Attention to fixation was modeled as a Gaussian at fixation (AF_{fix}). Attention to the bar stimulus was modeled as all unique bar stimuli (24 bar positions for each of 8 directions gives 192 unique bar stimuli) convolved with a Gaussian kernel (AF_{stim}). Both AF sizes varied in size separately, giving two free parameters. Specifically, the measured *Attend Fixation* pRF was divided by the AF_{fix} resulting in an estimate of the *SD*. Attention towards the stimulus was modeled by multiplying this *SD* by

the AF_{stim}, yielding one predicted *Attend Stimulus* pRF for each stimulus position. Each of these predicted pRFs were scaled back to maximum of 1, and subsequently summed. We then designated the peak of this summed profile as the predicted pRF center location in the *Attend Stimulus* condition. Formally, this is given by:

$$pRF_{stim}pos = argmax\left(\sum_{t=0}^{n}\left(\frac{(dm(t) * AF_{stim}) \cdot (pRF_{fix}/AF_{fix})}{max\left((dm(t) * AF_{stim}) \cdot (pRF_{fix}/AF_{fix})\right)}\right)\right) \quad (2)$$

where dm is a design matrix reflecting stimulus position at timepoint t, and n is the amount of timepoints. The predicted pRF shift was taken to run from the measured *Attend Fixation* pRF position towards this predicted *Attend Stimulus* center location. The AF sizes were determined at an ROI level, thus assuming that attention influenced all pRFs within an ROI similarly, while possibly varying between ROIs. We minimized the L2 distance between the predicted and measured pRF shift in the 64 bin quadrant visual field format of Figure 4B. We estimated Attention Field sizes in a 20 x 20 evenly spaced grid, where the AF towards fixation varied between 1.5-2.5 dva, and the AF towards the stimulus varied between 0.6-1.6 dva (i.e. 0.05 dva precision). The convolution between the stimulus and the AF_{stim} resulted in AF_{stim} width to be 0.9 (the bar stimulus width) larger than the AF_{stim} itself. These parameter ranges therefore result in equal effective AF sizes. Reported sizes are the standard deviation of the 2D Gaussians, with 0.9 (the bar width) added to AF_{stim} sizes. In order to estimate changes in the AF_{stim} size between the *Attend Color* and *Attend Speed* conditions AF_{fix} size was fixed at the value found in the *Attend Stimulus* condition. For this, a 100 element grid was used to estimate AF_{stim} size at high spatial resolution (0.01 dva). In order to provide an estimate of variance, AF sizes were determined through a jackknife procedure leaving out one participant per fold and fitting on pooled pRFs of remaining participants. Confidence intervals were then generated by bootstrapping over the resulting 5 estimates of AF size.

Gaze data processing

Gaze data was cleaned by linearly interpolating blinks detected by the EyeLink software. Transient occasions in which the tracker lost the pupil due to partial occlusion by

the eyelid leading to high-frequency, high-amplitude signal components were detected and corrected as follows. Pupil size was first high-pass filtered at 10 Hz (the pupil impulse response function is a low-pass filter with a cutoff below 10 Hz (Knapen et al., 2016; Korn and Bach, 2016)), after which those time-points in which the acceleration of pupil size was greater than 10^5 mm/s, and their neighbours within 5 s, were replaced with NaN values. Drift correction was performed within each bar-pass by subtracting the median gaze position. All gaze positions were rotated to the direction of bar movement, after which we analyzed the mean and variance (sd) of the component in the direction of bar movement (i.e. the component relevant for the pRF measurement).

Results

We first characterize the pattern of pRF parameter changes that resulted from the differential allocation of spatial attention (i.e. either toward fixation or the moving bar stimulus). Then, we investigate how feature-based attention (i.e. either towards color or temporal frequency changes in the bar) modulated these pRF changes and considered how this affected the distribution of color compared to temporal frequency preferences across the visual field. Finally, we verify that the changes in pRF parameters between attention conditions are not due to any differences in behavioral difficulty or fixation accuracy.

Spatial attention

Figure 2A shows voxels' *Attention to Fixation* location preferences, by depicting color-coded polar angle coordinates on an inflated cortical surface for one example participant's right hemisphere. We examined the relation between pRF eccentricity and size within each of the retinotopic regions, and performed further analyses on those regions that showed clear progressions of polar angle on the surface as well as positive size-eccentricity relations in all participants, as shown in Figure 2B. In addition we created a *combined* ROI that pooled voxels across selected ROIs, in order to evaluate pRF changes regardless of region of interest (ROI).

In order to quantify pRF changes resulting from differential allocation of spatial atten-

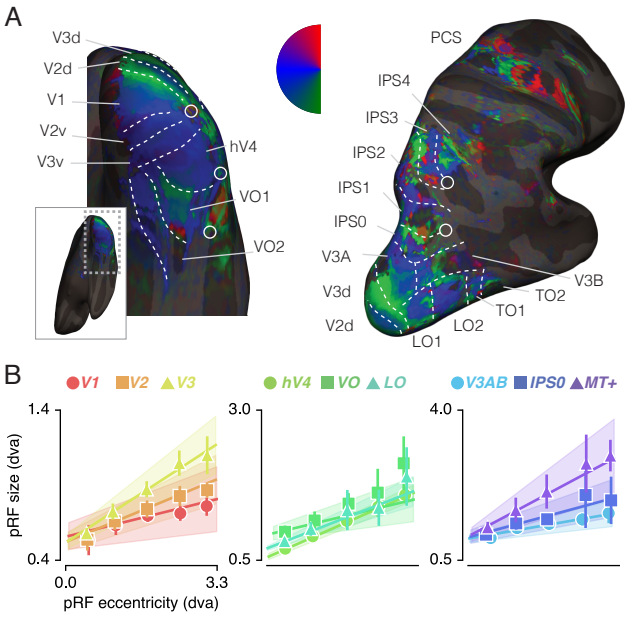

Figure 2: ROI definition A. *Attention to Fixation* pRF polar angle maps for an example participant with retinotopic areas up to the intra-parietal sulcus defined by hand. B. *Attention to Fixation* pRF size as a function of eccentricity for all areas that showed robust relationships across all participants. All error bars and shaded error regions denote 95% CI of data and linear fits respectively over participants.

tion we created an *Attention to Stimulus* condition by averaging pRF parameters between the *Attention to Color* and *Attention to TF* conditions. To inspect how spatial attention affected pRF positions, we plotted a vector from the *Attend Fixation* to the *Attend Stimulus* pRF position (Figure 3A). Visual inspection of these pRF position shifts shows both increasing shift magnitude up the visual hierarchy and shifts occuring mainly along the radial dimension (i.e. towards or away from the fovea). To quantify the direction of pRF shifts we computed the ratio of shifts in the radial, horizontal, and vertical directions. Figure 3C shows that pRF shifts are best described by shifts in the radial dimension in all ROIs (i.e. changes in eccentricity; bootstrap distribution of paired differences does not include zero with FDR corrected $p < .01$, see Figure 8). Additionally, Figure 3C reveals that changes of pRF horizontal location consistently better describe the overall shifts than do changes of pRF vertical location in all ROIs except V1/2/3 (bootstrap distribution of paired differences do not include zero with FDR corrected $p < .05$, see Figure 8). Figure 3D is intended to ease interpretation of these results. It depicts how different hypotheses regarding the underlying directionality of pRF shifts (i.e. horizontal, vertical, or radial) translate into changes in measured pRF x, y, and eccentricity as a function of polar angle. For example, if pRFs shift primarily in the radial direction (right column, Figure 3D), this would mean that pRF x and y shifts correlate with polar angle, whereas pRF eccentricity changes would be independent of polar angle. Figure 3D, right column, shows that the data (*combined* ROI) indeed correspond most to the radial shift hypothesis. Correspondingly, we found that correlations with polar angle were stronger for both horizontal and vertical position shifts compared to radial position shifts in the *combined* ROI (bootstrapped distribution of correlation differences differed from 0 for both measures with FDR corrected $p < .001$, $N = 11066$). This pattern of results indicates that spatial attention to the visual stimulus induced radial (foveopetal/foveofugal) pRF shifts. One likely cause for the predominance of horizontal vs. vertical shifts we report above is the overrepresentation of the horizontal meridian throughout the visual hierarchy at both subcortical (Schneider et al., 2004) and cortical (Swisher et al., 2007) levels. This overrepresentation of the horizontal meridian is also clearly present in our data (Rayleigh tests for non-uniformity in ROIs separately, all FDR corrected $ps < .001$, see Figure 9). This non-uniformity in visual field coverage causes shifts that occur exclusively in the radial

dimension to appear as a dominance of horizontal compared to vertical shifts when averaging over the visual field.

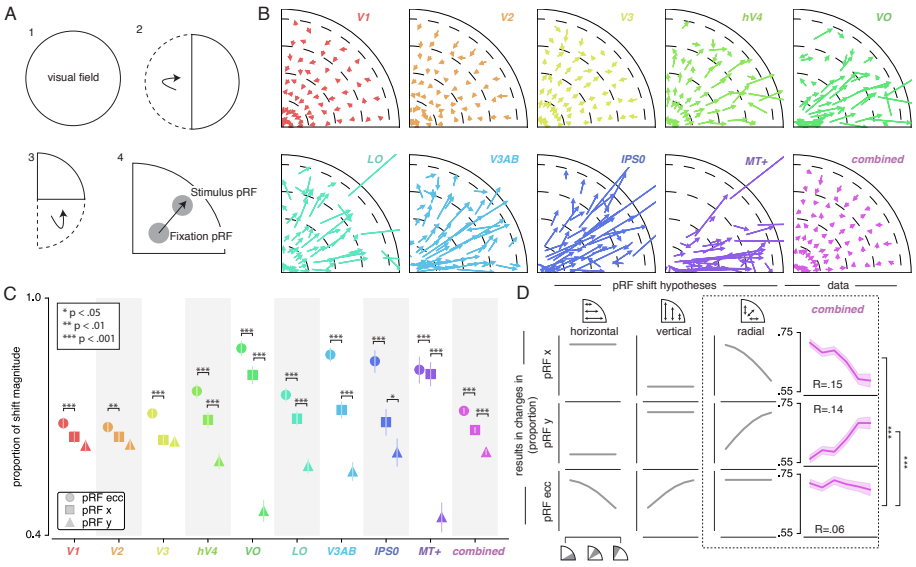

Figure 3: Effect of attention on pRF position. A. Plotting strategy. For pRF shift visualizations, all pRF positions are mirrored into one quadrant of the visual field. Then, vectors representing the shift of pRF centers between conditions were drawn from the *Attention to Fixation* pRF position to the *Attention to Stimulus* pRF position. B. Shift vectors as described in A. pRF shift magnitude increased up the visual hierarchy, and shifts appear to occur mainly in the radial direction (i.e. changes in pRF eccentricity). Dotted lines demarcate eccentricity bins used in subsequent analyses. C. Changes in pRF position in the horizontal, vertical, and radial directions as a proportion of the length of the shift vectors, as depicted in B. The magnitude of pRF shifts is consistently best described by changes in pRF eccentricity. D. pRF x, y and eccentricity position shifts plotted as a function of polar angle, for different shift direction hypotheses. The data closely matches the radial shift direction hypothesis, showing strongest pRF x shifts close to the horizontal meridian, strongest pRF y shifts close to the vertical meridian and no polar angle dependence on pRF eccentricity shifts. In C and D, single, double, and triple asterisks indicate significantly differences of FDR corrected $p < .05$, $< .01$ and $< .001$ respectively.

To further inspect the attention-induced radial shifts described above, we plotted the difference between *Attention to Stimulus* and *Attention to Fixation* pRF eccentricity for each of four *Attention to Fixation* pRF eccentricity bins (Figure 4A). The *combined* ROI shows that overall, central pRFs shifted away from the fovea, while peripheral pRFs shifted towards the fovea (bootstrap distribution does not include 0 with FDR corrected $p < .05$, see Figure 10). These outwards shifting central pRFs are found in all other ROIs except

V1 and V2, whereas the inwards shifting peripheral pRFs are also present in V1, V2 and V3.

In addition to pRF position changes, we also inspected changes in pRF size induced by differences in spatial attention as a function of *Attention to Fixation* pRF eccentricity (Figure 4B). Overall, central pRFs increased in size, while peripheral pRFs decreased in size (bootstrap distribution does not include 0 with FDR corrected $p < .05$; *combined* ROI, see Figure11). These expanding central pRFs were present in all ROIs except V2/3, whereas shrinking peripheral pRFs were found in all ROIs except V1, MT+ and IPS0. Overall, this pattern of results is strikingly similar to the changes in pRF eccentricity described above. In fact, the changes in pRF size and eccentricity were strongly correlated on a voxel to voxel level in all ROIs (Pearson R between .11 and .82, all bootstrapped distributions differed from 0 with $p < .001$; Figure 4C; Table 11). Together, these results showed that attention to the stimulus caused central pRFs to shift away from the fovea and increase in size, whereas peripheral pRFs shifted towards the fovea and decreased in size.

Formal account for observed pattern of pRF shifts

In order to provide a parsimonious explanation for the complex pattern of pRF shifts described above, we modeled our results using a multiplicative Gaussian interaction model (Womelsdorf et al., 2008; Klein et al., 2014), adapted to work in attentional conditions where attention shifted over space as a function of time (see Methods). Briefly, this approach modeled the effect of spatial attention on pRFs as the multiplication between two 2D Gaussians, one representing the Stimulus Drive (SD, i.e. the pRF outside the influence of attention), and another the Attention Field (AF, i.e. the location and spread of spatial attention). The smaller the AF, the stronger the effect on the SD. We modeled both the effect of attention to fixation and towards the bar stimulus, yielding two AF sizes. Figure 5A provides a schematic overview of the modeling procedure. The observed and predicted pRF shifts are depicted in Figure 5B, illustrating that the model accurately reproduced both the dominant radial shift direction and the direction of shift along this axis (i.e. central pRFs shifting towards the periphery and peripheral pRFs shift towards the fovea). To

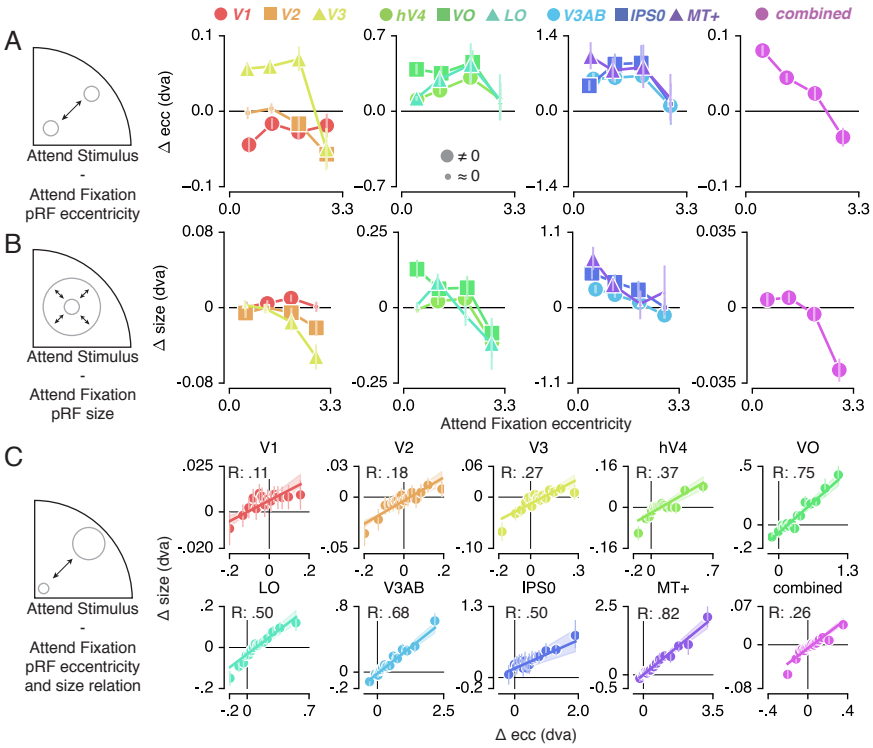

Figure 4: Effect of attention on pRF eccentricity and size. Difference between *Attention to Stimulus* and *Attention to Fixation* pRF eccentricity (A) and size (B) as a function of *Attention to Fixation* eccentricity. Overall, central pRFs tend to shift away from the fovea and increase in size, while peripheral pRFs tend to shift towards the fovea and decrease in sizes. C. Changes in pRF eccentricity and size were correlated on a voxel-by-voxel basis for all ROIs. Each markers' errorbar denotes 95% CI of data over voxels. In A and B, Markers are reduced in size when bootstrapped distributions differ from 0 with FDR corrected $p < .05$. In C, shaded error regions denote 95% CI of linear fit parameters over voxels.

summarize model performance across ROIs, we next plotted the predicted change in eccentricity as a function of eccentricity (i.e. the dominant pRF shift direction; Figure 5C). This showed that the model was able to capture differences in eccentricity change profiles across ROIs using very similar AF sizes (Figure 5D). Differences in observed eccentricity shift direction and magnitude over ROIs thus mainly depended on differences in spatial sampling between ROIs, rather than on differential properties of the attentional influence. Together, this shows that the relatively complex nature of the observed pRF shift patterns can be explained by a multiplicative Gaussian interaction process in which the influence of attention is similar across the visual hierarchy.

Feature-based attention

Having established the pattern of changes in spatial sampling (i.e. changes in pRF size and eccentricity) resulting from differential allocation of spatial attention, we next examined 1. how this pattern was modulated by differential feature-based attention, and 2. how this affected the distribution of feature preferences across the visual field. Figure 6A shows how pRF eccentricity and size are differentially affected by attending color or temporal frequency within the stimulus for the *combined* ROI. This illustrates that while both tasks caused similar pRF changes, these effects were generally more pronounced when attending color. In addition, we found smaller stimulus Attention Field sizes in the *Attend Color* compared to the *Attend TF* condition (Figure 6B; bootstrapped distribution of AF size difference over ROIs ($N = 9$) larger than 0 with $p < .001$). In order to quantify this observation per voxel, we combined changes in pRF eccentricity and size (as these were highly correlated (Figure 4C)) to form one robust index of the degree to which spatial attention resampled visual space (see Methods). Next, we computed how feature-based attention modulated this index (quantified as an attentional modulation index (AMI)). To examine the effects of this spatial resampling on the distribution of feature preferences across the visual field, we estimated in a separate experiment the difference in response amplitude to the presence of color and temporal frequency within a full-field stimulus (see Methods). Higher values of feature preference indicate greater preference for color compared to TF. Figure 6C displays feature-based AMI as a function of feature preference, averaged per

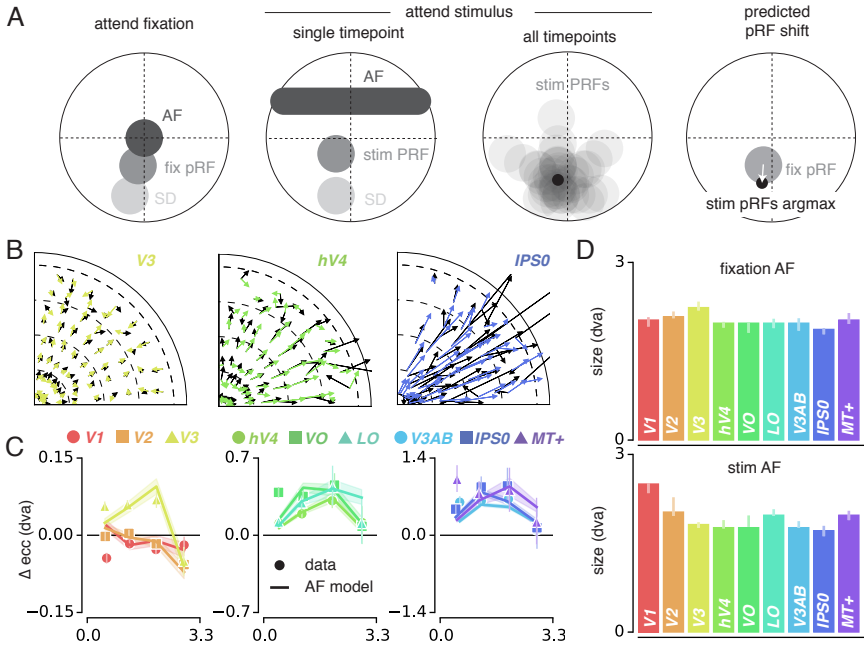

Figure 5: Attention Field (AF) modeling showed that the changes in pRF position can be described by a Gaussian interaction process. A. Schematic overview of modeling procedure. The Stimulus Drive (SD) was estimated by dividing the measured *Attend Fixation* pRF by an AF at fixation. Attention towards the bar stimulus at a given timepoint was modeled as the multiplication of the estimated SD with the bar stimulus at that timepoint convolved with an AF. These predicted *Attend Stimulus* pRFs were normalized to peak of 1 and summed over all timepoints. The maximum position of this profile was taken as the predicted *Attend Stimulus* pRF position. The predicted pRF shift ran from the measured *Attend Fixation* pRF towards the predicted *Attend Stimulus* position. B. Example predicted and measured pRF shifts for V3, hV4 and IPS0. Dotted lines demarcate the eccentricity bins used in C. C. Model performance summarized as the observed and predicted changes in pRF eccentricity (the main pRF shift direction) as a function of eccentricity. Markers depict data and lines the corresponding AF model fit. D. AF sizes are comparable across ROIs. Error bars denote 95% CIs over voxels in C, and over jackknife folds in D and E. Plotting conventions as in 3.

ROI. We first describe the distributions of each of these measures separately, after which we investigate their interaction.

The y-axis shows positive AMIs in all ROIs (bootstrap distribution does not include zero with $p < .05$, see Figure 13). This indicates that attending color compared to TF changes in the bar stimulus produced stronger spatial resampling. The x-axis of Figure 6C shows the strongest preference for TF compared to color in areas MT+ and V1, and strongest preference for color compared to TF in areas V4 and VO. This agrees with established specializations of these areas (Liu and Wandell, 2005; Brouwer and Heeger, 2009, 2013). Regardless of these large variations in relative feature preferences, average feature AMI was roughly equal in these ROIs. In fact, there was no correlation between feature preference and feature-based AMI across ROIs ($R = -.07$, $p = .841$, $N = 9$). This shows that the changes in spatial sampling that resulted from differential allocation of feature-based attention were uniform across the visual system, irrespective of the average difference in preference for these features in each ROI.

The purpose of this study was to establish whether changes in the sampling of visual space as induced by varying spatial attention leads to a redistribution of feature-processing resources across the visual field. Furthermore, our goal was to investigate whether such changes are modulated by feature-based attention. In line with an established specialization for temporal compared to color information in the periphery (Hartmann et al., 1979; Curcio et al., 1990; Azzopardi et al., 1999; Brewer et al., 2005; Lui et al., 2007; Hansen et al., 2009; Yu et al., 2010), we find a gradient of decreasing color compared to temporal frequency preference with increasing eccentricity. This is evidenced by negative correlations between feature preference and *Attend Fixation* pRF eccentricity in all but one ROIs (bootstrap distribution of Spearman rho below 0, FDR corrected ps $< .05$ except in IPS0; black circles Figure 6C; see Figure 10). We next examined whether spatial resampling as induced by spatial attention mitigated this uneven distribution of relative feature preferences across the visual field. Indeed, we find reduced negative correlations between feature preference and pRF eccentricity in the *Attend Stimulus* compared to the *Attend Fixation* condition in most ROIs (Figure 6C, circles and upwards triangles respectively; bootstrap distribution of Spearman rho differences differed from 0 with FDR corrected $p < .05$ except in V1 and MT+, see Figure 14). In addition, we found further re-

ductions in the negative correlations between feature preference and pRF eccentricity in the *Attend Color* compared to the *Attend TF* condition in most ROIs (Figure 6C, squares and downward triangles respectively; bootstrap distribution of correlation differences different from 0 with FDR corrected $p < .05$ except in V2 and hV4, see Figure 14). However, in V1 we found the opposite; correlation between feature preference and pRF eccentricity here was more negative when attending color compared to TF. This pattern of results can be understood from the average changes in pRF eccentricity across ROIs (see Figure 4A). The negative correlation between *Attend Fixation* pRF eccentricity and feature preference indicated that color-preferring pRFs were predominantly positioned in the central portion of the visual field. As attending the stimulus decreased pRF eccentricities in V1, this further enhanced the concentration of relative color-preferring pRFs around the fovea. Conversely, in higher order ROIs attending the stimulus increased central pRFs' eccentricity, thereby redistributing relative color-preferring central pRFs towards the periphery. Together, these results show that feature-based attention modulated the changes in spatial sampling that resulted from varying spatial attention. This in turn changed the distribution of relative feature preferences across the visual field.

Task and Fixation Performance

Finally, we checked whether the pRF results were not affected by differences in fixation accuracy or behavioral performance (see Figure 7). To provide evidence in favor of these null hypothesis, we performed JZL Bayes factor analyses (using JASP; Love et al. (2015)). We rotated recorded eye position to the direction of bar movement and computed the median and standard deviation of position along this dimension per bar position (Figure 7B). We next setup a model including the factor of attention condition (3 levels), bar position (24 levels), and their interaction. We found that when predicting gaze position, the evidence was in favor of the null hypothesis with a Bayes factor of 18620. When predicting gaze variability however, we found evidence against the null hypothesis with a Bayes factor of 5.980. Evidence for including each of the factors (condition, bar position, and their interaction) into the model returned Bayes factors of 0.713, 547.193 and 0.017 respectively. This showed that although bar position influenced gaze variability, it did

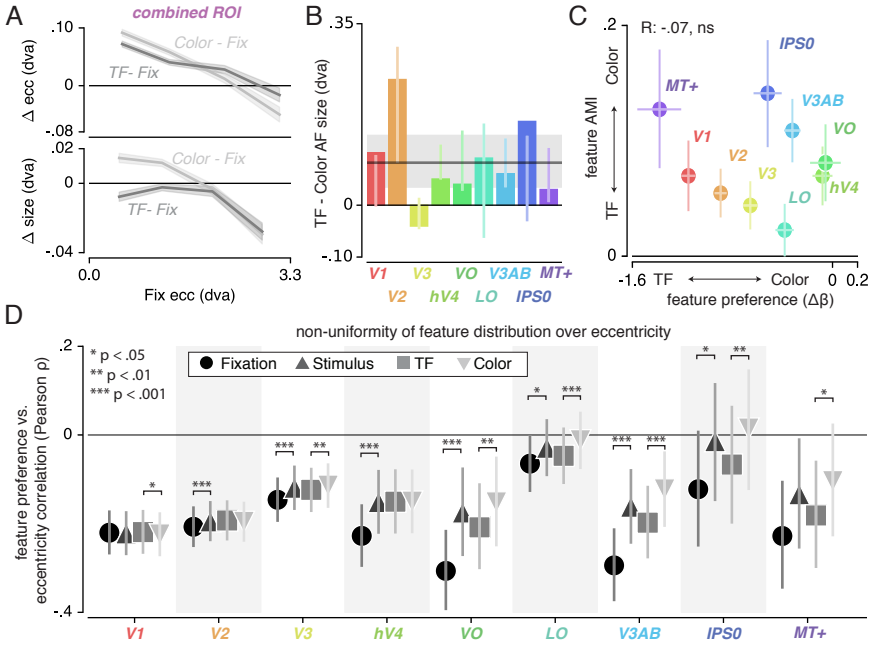

Figure 6: Feature-based modulation of pRF changes induced by differential spatial attention, and its relation to feature preference. A. Differences in pRF eccentricity and size relative to the *Attention to Fixation* condition, for both the *Attention to Color* and *Attention to TF* condition separately. The changes in both eccentricity and size are more pronounced when attending changes in color versus TF changes in the bar. B. This is mirrored by generally smaller AFs towards the stimulus in the *Attend Color* compared to *Attend TF* conditions. Black horizontal line and shaded area indicates average and 95% CI of AF size difference over ROIs. C. The y-axis displays feature AMI, which increases when pRF modulations (size and eccentricity changes combined, see Methods) are greater when attending color compared to TF in the bar stimulus. The x-axis displays feature preference, which inreases wiht higher color compared to TF preference. pRF modulations were greater when attending color, which was unrelated to feature preference. D. Distribution of feature preference across eccentricity. Negative correlations between feature preference and eccentricity indicate low relative preference for color compared to TF in the periphery. This negative relation is reduced most when attending color in the stimulus in most ROIs, but slightly increased in V1. In A, C, and D errorbars denote 95% CI over voxels, in B, error bars denote 95% CI over jackknife folds over subjects. Note that central parameter estimates do not neccesarily include error bars as a consequence of the resampling procedure.

not do so differently between attention conditions. Using a similar approach, we then tested whether a model including attention condition (3 levels) and stimulus eccentricity (3 levels) influenced behavioral performance (Figure 7A). This returned evidence for the null hypothesis with a Bayes factor of 6.25. Together, this showed that any differences in pRF parameters between conditions cannot be explained by either fixation accuracy or behavioral difficulty.

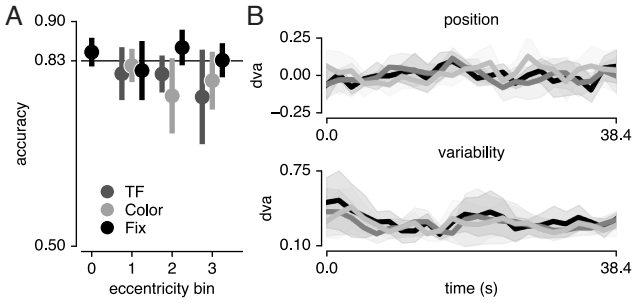

Figure 7: Task and Fixation performance A. Behavioral Performance. Behavioral accuracy per attention condition and per bar stimulus eccentricity bin. Horizontal line denotes Quest target of 83%; chance level was 50%. B. Median (top pannel) and standard deviation (bottom pannel) gaze position in the direction of bar movement per bar position. Error bars denote 95% CI across 5 participants.

Discussion

We investigated how feature-based and spatial attention together change the sampling of visual space, and how this altered the distribution of feature preferences across the visual field. We find that directing spatial attention towards a moving bar stimulus altered the eccentricity and size of pRFs in concert. Attending color changes within this stimulus induced stronger pRF changes compared to attending temporal frequency changes, irrespective of whether a visual region as a whole was activated more by color or by temporal frequency. In addition, these changes in spatial sampling lead to concurrent redistributions of color relative to temporal frequency preferences across the visual field.

We found that directing spatial attention towards the moving bar stimulus instead of towards fixation changed pRF eccentricity and size in concert. Specifically, both pRF size

and eccentricity decreased on average in V1 and V2, but increased on average in other visual areas. This closely matches data from a study where participants attended non-moving, peripheral stimuli versus fixation (Kay et al., 2015), which reported reductions in pRF size and eccentricity in V1 and V2, but increases in higher order areas. This indicates that our results are not specific for attention towards a moving stimulus, but are general for attending the periphery instead of fixation. In addition, we showed that the pattern of pRF shifts we observed is well described by an Attention Field model. In agreement with earlier reports (Klein et al., 2014; Puckett and DeYoe, 2015), we found that the best-fitting model implemented comparable Attention Field sizes for all visual ROIs. This strongly points to spatial attention being implemented as a global influence across visual cortex. Thus, reductions in pRF eccentricity in V1 and V2 can be ascribed to their distinct spatial sampling, i.e. pRFs being smaller in those regions. Of interest, despite the broad correspondence between model fits and data, in these lowest cortical visual ROIs the model fails to predict that stimulus-based attention decreased the eccentricity of the most foveal pRFs in V1. Two recent studies showed that in early visual areas, spatial attention shifted pRFs away from the attended location, but towards the attended location in higher visual areas (Haas et al., 2014; Vo et al., 2017). Other studies showed that in precisely these visual regions, both the pRF and the attention field comprise a suppressive surround in addition to their positive peak (Zuiderbaan et al., 2012; Puckett and DeYoe, 2015). We leave the question whether these suppressive surrounds explain such repulsive shifts in lower visual cortex for future research.

pRF size and eccentricity also changed in concert within visual areas. Directing spatial attention towards the moving bar stimulus relative to attending fixation increased eccentricity and size in central pRFs, and decreased eccentricity and size in peripheral pRFs. This finding supports the resolution hypothesis of attention (Anton-Erxleben and Carrasco, 2013), which posits that spatial attention acts to reduce resolution differences between the fovea and periphery. Yet, the functional implication of pRF size changes was recently questioned, as stimulus encoding fidelity was shown to be affected by pRF position and not by size changes (Vo et al., 2017). Alternatively, it is possible that changes in pRF size are an indirect consequence of pRF eccentricity changes. Cortical network models posit that spatial attention modifies receptive fields by temporarily altering feed-

back originating from receptive fields at the attended location (either through lateral or feedback connections, see Compte and Wang (2006)). As receptive field size scales with eccentricity, attention directed towards the periphery will increase feedback from large peripheral receptive fields towards small central receptive fields and vice versa.

In all visual areas, directing attention to the color content of the stimulus evoked greater spatial pRF changes compared to directing attention to the temporal frequency content of the stimulus. This agreed with generally smaller Attention Fields when attending color compared to TF. This prominence of attention to color was irrespective of the average relative sensitivity to changes in color vs. temporal frequency within that visual region. In other words, while MT+ and V4 differed greatly in their relative feature preference, both areas showed comparable pRF changes resulting from differences in feature-based attention. On the one hand, this stands in apparent contrast with previous studies showing that feature-based attention selectively enhanced responses in the cortical areas specialized in processing that feature (Corbetta et al., 1990; Chawla et al., 1999; O'Craven et al., 1999; Schoenfeld et al., 2007; Baldauf and Desimone, 2014). On the other hand, our findings agree with recent studies, showing that feature-based attentional enhancements are not restricted to the area most sensitive to that feature (Çukur et al., 2013; Schoenfeld et al., 2014; Kay and Yeatman, 2017).

We found that the preference of voxels in terms of color or temporal frequency correlated negatively with their eccentricity, in most visual regions. This agrees with decreasing ratios of color-sensitive cones over temporally sensitive rods with increasing eccentricity (Curcio et al., 1990). In addition, input to foveal areas of V1 are dominated by color-opponency carrying parvocellular inputs from LGN (Azzopardi et al., 1999). Correspondingly, color selectivity only exists in foveal areas of hV4 and VO (Brewer et al., 2005), whereas for temporal frequency, bandwidth is constant and frequency tuning increases over eccentricity in macaque V1 (Yu et al., 2010) and MT+ (Lui et al., 2007). This is mirrored by behavioral studies, showing that chromatic detection and hue discrimination is best near the fovea (Hansen et al., 2009), whereas the optimal flicker fusion frequency increases with eccentricity (Hartmann et al., 1979). Interestingly, our findings showed that this differential distribution of feature preferences across the visual field is not fixed, but is instead altered by the combined application of spatial and feature-based

attention. In higher-level visual cortex attending color in the stimulus greatly alleviated the relatively low preference for color in the periphery. Thus, the spatial distribution of feature preferences was adapted to meet task demands in higher visual regions (i.e. detecting color changes in the relatively peripheral bar stimulus). In V1 however, attending color in the stimulus slightly reduced preference for color in the periphery. This pattern of results depends on the average change in pRF eccentricity across visual areas. Whereas pRFs shifted towards the fovea on average in V1, pRFs shifted outwards on average in higher visual regions. Our attention field modeling results show that feature-based attention modulated the strength of spatial attention induced pRF changes across the visual system simultaneously by decreasing Attention Field size. This in turn improved the distribution of feature preferences across the visual field for task demands in higher visual areas.

By using a full encoding model only for the spatial dimension and not feature preferences, we leverage the distributed nature of spatial representation for our experimental question. As it is possible to track an object through feature space (Blaser et al., 2000), this leaves open the question whether our findings would translate to the domain of other visual features. Findings in more high-level domains indicate that attentionally induced changes in the representation of semantic information occur throughout cortex as well (Çukur et al., 2013).

We show for the first time that spatial and feature-based attention interact when attending a specific feature at a particular location. Electrophysiological studies investigating the relation between spatial and feature-based attention conclude that their contributions on firing rates are independent (Hayden and Gallant, 2009; Ibos and Freedman, 2016). Additionally, one study showed that shifts in spectral tuning curves induced by feature-based attention are independent of spatial attention (David et al., 2008). We add to this the observation that changes in spatial tuning induced by spatial attention are modulated by the attended feature and the distribution of feature preference over the visual field.

An important remaining question concerns the source of the interactions between feature based and spatial attention. Signals of spatial selection are thought to originate from a network of frontal and parietal areas, identified using fMRI (Shulman, 2002; Silver

et al., 2005; Sprague and Serences, 2013; Kay and Yeatman, 2017), and electrophysiology (Moore and Armstrong, 2003; Gregoriou et al., 2009). In macaques, an area on the ventral prearcuate gyrus (VPA) was recently shown to contain selectivity to both visual features and visual space (Bichot et al., 2015). This region preceded visual cortex in signaling feature selection and endowed the frontal eye fields with feature selectivity. Furthermore, deactivation of the VPA mitigated feature-based attentional performance. This suggests a central role for the VPA in controlling interactions between feature-based and spatial attention. Indeed, signals of feature selection in humans have been localized to the inferior frontal junction (IFJ), a likely human VPA homologue (Zanto et al. (2010); Baldauf and Desimone (2014)).

In sum, we showed that resampling of visual space is not only determined by the attended location, but also depends on the sensitivity for an attended feature at that location. Together, our results further establish the highly flexible nature of the brains' encoding of sensory information to meet task demands (Rosenholtz, 2016).

direction of pRF shift

	ecc > x		x > y	
	N	p	N	p
V1	2176	<.001***	2176	.101
V2	2752	.002**	2752	.108
V3	2318	<.001***	2320	.771
hV4	1201	<.001***	1201	<.001***
VO	573	<.001***	582	<.001***
LO	1394	<.001***	1397	<.001***
V3AB	873	<.001***	880	<.001***
IPS0	313	<.001***	313	.022*
MT+	306	<.001***	325	<.001***
combined	11060	<.001***	11066	<.001***

Figure 8: Statistics corresponding to Figure 3C. P-values reflect proportion of bootstrapped shift ratios different from 0. Single, double and triple asterisks indicate FDR corrected significance of <.05, <.01 and <.001 respectively. FDR correction performed over all p-values in this table simultaneously.

Rayleigh test for non-uniformity

	N	z	p
V1	2176	66.8476	<.001***
V2	2754	51.9041	<.001***
V3	2322	63.7037	<.001***
hV4	1201	50.4177	<.001***
VO	582	116.5634	<.001***
LO	1405	40.9949	<.001***
V3AB	883	32.5543	<.001***
IPS0	316	56.9459	<.001***
MT+	328	119.0523	<.001***
combined	11084	431.5976	<.001***

Figure 9: Statistics corresponding to Figure 3. P-values reflect whether pRFs are distributed non-uniformly over polar angle (Rayleigh test). Triple asterisks indicate FDR corrected significance of <.001. FDR correction performed over all p-values in this table simultaneously.

changes in pRF eccentricity different from 0

ecc bin	1		2		3		4	
	N	p	N	p	N	p	N	p
V1	509	<.001***	749	<.001***	595	<.001***	323	.012*
V2	862	.935	931	.152	616	<.001***	343	<.001***
V3	920	<.001***	747	<.001***	427	<.001***	226	<.001***
hV4	693	<.001***	359	<.001***	110	<.001***	39	0.044
VO	313	<.001***	162	<.001***	71	<.001***	36	.308
LO	1047	<.001***	263	<.001***	56	<.001***	31	.263
V3AB	220	<.001***	348	<.001***	199	<.001***	113	.016*
IPS0	170	<.001***	86	<.001***	36	<.001***	21	.448
MT+	186	<.001***	103	<.001***	18	<.001***	18	.230
combined	4700	<.001***	3400	<.001***	1929	<.001***	1037	<.001***

Figure 10: Statistics corresponding to Figure 4A. P-values reflect whether bootstrapped distribution is different from 0, for each ROI and each eccentricity bin. Single, double and triple asterisks indicate FDR corrected significance of <.05, <.01 and <.001 respectively. FDR correction performed over all p-values in this table simultaneously.

changes in pRF size different from 0

ecc bin	1		2		3		4	
	N	p	N	p	N	p	N	p
V1	509	.624	749	<.001***	595	<.001***	323	.661
V2	862	.007*	931	.878	616	.012*	343	<.001***
V3	920	.236	747	.609	427	<.001***	226	<.001***
hV4	693	.040	359	<.001***	110	.012*	39	<.001***
VO	313	<.001***	162	<.001***	71	<.001***	36	<.001***
LO	1047	.059	263	<.001***	56	.109	31	.007*
V3AB	220	<.001***	348	<.001***	199	<.001***	113	<.001***
IPS0	170	<.001***	86	<.001***	36	<.001***	21	.990
MT+	186	<.001***	103	<.001***	18	.533	18	.132
combined	4700	.005**	3400	<.001***	1929	.034*	1037	<.001***

Figure 11: Statistics corresponding to Figure 4B. P-values reflect whether bootstrapped distribution is different from 0, for each ROI and each eccentricity bin. Single, double and triple asterisks indicate FDR corrected significance of <.05, <.01 and <.001 respectively. FDR correction performed over all p-values in this table simultaneously.

ecc and size change correlations

	N	p
V1	2115	<.001***
V2	2659	<.001***
V3	2186	<.001***
hV4	1106	<.001***
VO	541	<.001***
LO	1246	<.001***
V3AB	841	<.001***
IPS0	285	<.001***
MT+	303	<.001***
combined	9996	<.001***

Figure 12: Statistics corresponding to Figure 4C. P-values are uncorrected two-tailed tests whether bootstrapped distribution of correlations is different from 0. Triple asterisks indicate FDR corrected significance of <.001 respectively. FDR correction performed over all p-values in this table simultaneously.

feature AMI different from 0

	N	p
V1	1529	<.001***
V2	2055	<.001***
V3	1684	<.001***
hV4	826	<.001***
VO	448	<.001***
LO	968	.045*
V3AB	678	<.001***
IPS0	231	<.001***
MT+	242	<.001***

Figure 13: Statistics corresponding to Figure 6B. P-values are uncorrected two-tailed tests whether bootstrapped distribution is different from 0. Triple asterisks indicate FDR corrected significance of <.001 respectively. FDR correction performed over all p-values in this table simultaneously. < .01.

feature pref and pRF ecc correlation

		fix	stim-fix	color-speed
	N	p	p	p
V1	1604	<.001***	.603	.026*
V2	2154	<.001***	<.001***	.119
V3	1783	<.001***	<.001***	.003**
hV4	875	<.001***	<.001***	.980
VO	465	<.001***	<.001***	.001**
LO	1010	.038*	.016*	<.001***
V3AB	703	<.001***	<.001***	<.001***
IPS0	235	.063	.016*	.005**
MT+	251	<.001***	.137	.007*
combined	7921	<.001***	<.001***	<.001***

Figure 14: Statistics corresponding to Figure 6C. P-values are uncorrected two-tailed tests whether bootstrapped distribution is different from 0. Single, double and triple asterisks indicate FDR corrected significance of <.05, <.01 and <.001 respectively. Two separate FDR corrections were performed, one for the *Fix* column, and another for the latter two columns combined.

References

Anton-Erxleben K, Carrasco M (2013) Attentional enhancement of spatial resolution: linking behavioural and neurophysiological evidence. Nat Rev Neurosci 14:188–200.

Azzopardi P, Jones KE, Cowey A (1999) Uneven mapping of magnocellular and parvocellular projections from the lateral geniculate nucleus to the striate cortex in the macaque monkey. Vision Res 39:2179–2189.

Baldauf D, Desimone R (2014) Neural mechanisms of object-based attention. Science 344:424–427.

Bichot NP, Heard MT, DeGennaro EM, Desimone R (2015) A source for feature-based attention in the prefrontal cortex. Neuron 88:832–844.

Blaser E, Pylyshyn ZW, Holcombe AO (2000) Tracking an object through feature space. Nature 408:196–199.

Brewer AA, Liu J, Wade AR, Wandell BA (2005) Visual field maps and stimulus selectivity in human ventral occipital cortex. Nat Neurosci 8:1102–1109.

Brouwer GJ, Heeger DJ (2009) Decoding and reconstructing color from responses in human visual cortex. J Neurosci 29:13992–14003.

Brouwer GJ, Heeger DJ (2013) Categorical clustering of the neural representation of color. J Neurosci 33:15454–15465.

Buračas GT, Boynton GM (2002) Efficient design of event-related fMRI experiments using M-sequences. NeuroImage 16:801–813.

Carrasco M, Yeshurun Y (1998) The contribution of covert attention to the set-size and eccentricity effects in visual search. J Exp Psychol Human 24:673–692.

Chawla D, Rees G, Friston KJ (1999) The physiological basis of attentional modulation in extrastriate visual areas. Nat Neurosci 2:671–676.

Compte A, Wang X-J (2006) Tuning curve shift by attention modulation in cortical neurons: a computational study of its mechanisms. Cereb Cortex 16:761–778.

Connor CE, Preddie DC, Gallant JL, Van Essen DC (1997) Spatial attention effects in macaque area V4. J Neurosci 17:3201–3214.

Corbetta M, Miezin FM, Dobmeyer S, Shulman GL, Petersen SE (1990) Attentional modulation of neural processing of shape, color, and velocity in humans. Science

248:1556–1559.

Curcio CA, Sloan KR, Kalina RE, Hendrickson AE (1990) Human photoreceptor topography. J Comp Neurol 292:497–523.

Çukur T, Nishimoto S, Huth AG, Gallant JL (2013) Attention during natural vision warps semantic representation across the human brain. Nat Neurosci 16:763–770.

David SV, Hayden BY, Mazer JA, Gallant JL (2008) Attention to stimulus features shifts spectral tuning of V4 neurons during natural vision. Neuron 59:509–521.

Dumoulin SO, Wandell BA (2008) Population receptive field estimates in human visual cortex. NeuroImage 39:647–660.

Found A, Müller HJ (1996) Searching for unknown feature targets on more than one dimension: Investigating a dimension-weighting account. Percept Psychophys 58:88–101.

Gregoriou GG, Gotts SJ, Zhou H, Desimone R (2009) High-frequency, long-range coupling between prefrontal and visual cortex during attention. Science 324:1207–1210.

Haas B de, Schwarzkopf DS, Anderson EJ, Rees G (2014) Perceptual load affects spatial tuning of neuronal populations in human early visual cortex. Curr Biol 24:R66–7.

Hansen T, Pracejus L, Gegenfurtner KR (2009) Color perception in the intermediate periphery of the visual field. J Vis 9:26.1–12.

Hartmann E, Lachenmayr B, Brettel H (1979) The peripheral critical flicker frequency. Vision Res 19:1019–1023.

Hayden BY, Gallant JL (2009) Combined effects of spatial and feature-based attention on responses of V4 neurons. Vision Res 49:1182–1187.

Ibos G, Freedman DJ (2016) Interaction between spatial and feature attention in posterior parietal cortex. Neuron 91:931–943.

Jehee JFM, Brady DK, Tong F (2011) Attention improves encoding of task-relevant features in the human visual cortex. J Neurosci 31:8210–8219.

Jenkinson M, Beckmann CF, Behrens TEJ, Woolrich MW, Smith SM (2012) FSL. NeuroImage 62:782–790.

Kay KN, Weiner KS, Grill-Spector K (2015) Attention reduces spatial uncertainty in human ventral temporal cortex. Curr Biol 25:595–600.

Kay KN, Yeatman JD (2017) Bottom-up and top-down computations in word- and

face-selective cortex. eLife 6:284.

Klein BP, Harvey BM, Dumoulin SO (2014) Attraction of position preference by spatial attention throughout human visual cortex. Neuron 84:227–237.

Knapen T, Gee JW de, Brascamp J, Nuiten S, Hoppenbrouwers S, Theeuwes J (2016) Cognitive and ocular factors jointly determine pupil responses under equiluminance. PLoS ONE 11:e0155574.

Korn CW, Bach DR (2016) A solid frame for the window on cognition: Modeling event-related pupil responses. J Vis 16:28.

Kumada T (2001) Feature-based control of attention: Evidence for two forms of dimension weighting. Percept Psychophys 63:698–708.

Lee S, Papanikolaou A, Logothetis NK, Smirnakis SM, Keliris GA (2013) A new method for estimating population receptive field topography in visual cortex. NeuroImage 81:144–157.

Liu J, Wandell BA (2005) Specializations for chromatic and temporal signals in human visual cortex. J Neurosci 25:3459–3468.

Love J, Selker R, Marsman M, Jamil T, Dropmann D (2015) Jasp (version 0.7)[computer software]. Amsterdam, The Netherlands: JASP Project.

Lui LL, Bourne JA, Rosa MGP (2007) Spatial and temporal frequency selectivity of neurons in the middle temporal visual area of new world monkeys (Callithrix jacchus). Eur J Neurosci 25:1780–1792.

Maunsell JHR, Treue S (2006) Feature-based attention in visual cortex. Trends Neurosci 29:317–322.

McAdams CJ, Maunsell J (2000) Attention to both space and feature modulates neuronal responses in macaque area V4. J Neurophysiol 83:1751–1755.

McKee SP, Nakayama K (1984) The detection of motion in the peripheral visual field. Vision Res 24:25–32.

Moore T, Armstrong KM (2003) Selective gating of visual signals by microstimulation of frontal cortex. Nature 421:370–373.

Müller MM, Andersen S, Trujillo NJ, Valdés-Sosa P, Malinowski P, Hillyard SA (2006) Feature-selective attention enhances color signals in early visual areas of the human brain.

Proc Natl Acad Sci USA 103:14250–14254.

O'Craven KM, Downing PE, Kanwisher N (1999) fMRI evidence for objects as the units of attentional selection. Nature 401:584–587.

Pedregosa F, Eickenberg M, Ciuciu P, Thirion B, Gramfort A (2015) Data-driven HRF estimation for encoding and decoding models. NeuroImage 104:209–220.

Peirce JW (2008) Generating stimuli for neuroscience using PsychoPy. Front Neuroinform 2:10.

Pestilli F, Carrasco M (2005) Attention enhances contrast sensitivity at cued and impairs it at uncued locations. Vision Res 45:1867–1875.

Posner MI, Snyder CR, Davidson BJ (1980) Attention and the detection of signals. J Exp Psychol 109:160–174.

Powell MJD (1964) An efficient method for finding the minimum of a function of several variables without calculating derivatives. Comput J 7:155–162.

Puckett AM, DeYoe EA (2015) The attentional field revealed by single-voxel modeling of fMRI time courses. J Neurosci 35:5030–5042.

Reynolds JH, Heeger DJ (2009) The normalization model of attention. Neuron 61:168–185.

Rosenholtz R (2016) Capabilities and limitations of peripheral vision. Annu Rev Vis Sci 2:437–457.

Rossi AF, Paradiso MA (1995) Feature-specific effects of selective visual-attention. Vision Res 35:621–634.

Saenz M, Buračas GT, Boynton GM (2002) Global effects of feature-based attention in human visual cortex. Nat Neurosci 5:631–632.

Saenz M, Buračas GT, Boynton GM (2003) Global feature-based attention for motion and color. Vision Res 43:629–637.

Savitzky A, Golay MJE (1964) Smoothing and differentiation of data by simplified least squares procedures. Anal Chem 36:1627–1639.

Schneider KA, Richter MC, Kastner S (2004) Retinotopic organization and functional subdivisions of the human lateral geniculate nucleus: a high-resolution functional magnetic resonance imaging study. J Neurosci 24:8975–8985.

Schoenfeld MA, Hopf J-M, Martinez A, Mai HM, Sattler C, Gasde A, Heinze H-J,

Hillyard SA (2007) Spatio-temporal analysis of feature-based attention. Cereb Cortex 17:2468–2477.

Schoenfeld MA, Hopf J-M, Merkel C, Heinze H-J, Hillyard SA (2014) Object-based attention involves the sequential activation of feature-specific cortical modules. Nat Neurosci 17:619–624.

Serences JT, Boynton GM (2007) Feature-based attentional modulations in the absence of direct visual stimulation. Neuron 55:301–312.

Sheremata SL, Silver MA (2015) Hemisphere-dependent attentional modulation of human parietal visual field representations. J Neurosci 35:508–517.

Shulman GL (2002) Two attentional processes in the parietal lobe. Cereb Cortex 12:1124–1131.

Silver MA, Ress D, Heeger DJ (2005) Topographic maps of visual spatial attention in human parietal cortex. J Neurophysiol 94:1358–1371.

Sprague TC, Serences JT (2013) Attention modulates spatial priority maps in the human occipital, parietal and frontal cortices. Nat Neurosci 16:1879–1887.

Swisher JD, Halko MA, Merabet LB, McMains SA, Somers DC (2007) Visual topography of human intraparietal sulcus. J Neurosci 27:5326–5337.

Theeuwes J, Van der Burg E (2007) The role of spatial and nonspatial information in visual selection. J Exp Psychol Human 33:1335–1351.

Treue S, Maunsell J (1999) Effects of attention on the processing of motion in macaque middle temporal and medial superior temporal visual cortical areas. J Neurosci 19:7591–7602.

Treue S, Maunsell JH (1996) Attentional modulation of visual motion processing in cortical areas MT and MST. Nature 382:539–541.

Vo VA, Sprague TC, Serences JT (2017) Spatial tuning shifts increase the discriminability and fidelity of population codes in visual cortex. J Neurosci 37:3386–3401.

Watson AB, Pelli DG (1983) Quest: A Bayesian adaptive psychometric method. Percept Psychophys 33:113–120.

Wegener D, Ehn F, Aurich MK, Galashan FO, Kreiter AK (2008) Feature-based attention and the suppression of non-relevant object features. Vision Res 48:2696–2707.

Wolfe JM, Butcher SJ, Lee C, Hyle M (2003) Changing your mind: On the contribu-

767 tions of top-down and bottom-up guidance in visual search for feature singletons. J Exp
768 Psychol Human 29:483–502.

769 Womelsdorf T, Anton-Erxleben K, Pieper F, Treue S (2006) Dynamic shifts of visual
770 receptive fields in cortical area MT by spatial attention. Nat Neurosci 9:1156–1160.

771 Womelsdorf T, Anton-Erxleben K, Treue S (2008) Receptive field shift and shrink-
772 age in macaque middle temporal area through attentional gain modulation. J Neurosci
773 28:8934–8944.

774 Yeshurun Y, Carrasco M (1999) Spatial attention improves performance in spatial
775 resolution tasks. Vision Res 39:293–306.

776 Yu HH, Verma R, Yang Y, Tibballs HA, Lui LL, Reser DH, Rosa MGP (2010) Spatial
777 and temporal frequency tuning in striate cortex: functional uniformity and specializa-
778 tions related to receptive field eccentricity. Eur J Neurosci 31:1043–1062.

779 Zanto TP, Rubens MT, Bollinger J, Gazzaley A (2010) Top-down modulation of visual
780 feature processing: the role of the inferior frontal junction. NeuroImage 53:736–745.

781 Zhang W, Luck SJ (2009) Feature-based attention modulates feedforward visual pro-
782 cessing. Nat Neurosci 12:24–25.

783 Zhou H, Desimone R (2011) Feature-based attention in the frontal eye field and area
784 V4 during visual search. Neuron 70:1205–1217.

785 Zuiderbaan W, Harvey BM, Dumoulin SO (2012) Modeling center-surround config-
786 urations in population receptive fields using fMRI. J Vis 12:10.